Submitted Manuscript

Applied Spectroscopy

www.s-a-s.org

Deep-Learning-Enabled High-Fidelity Absorbance Spectra from Distorted Dual-Comb Absorption Spectroscopy for Gas Quantification Analysis

Applied Spectroscopy
2024, Vol. 78(3) 310–320

DOI: 10.1177/00037028231226341
journals.sagepub.com/home/asp
Sage

Chao Huang[1], Tianyou Zhang[2], Xiangchen Kong[1], Yan Li[1], and Haoyun Wei[1]

Abstract

Dual-comb absorption spectroscopy has been a promising technique in laser spectroscopy due to its intrinsic advantages over broad spectral coverage, high resolution, high acquisition speed, and frequency accuracy. However, two primary challenges, including etalon effects and complex baseline extraction, still severely hinder its implementation in recovering absorbance spectra and subsequent quantification analysis. In this paper, we propose a deep learning enabled processing framework containing etalon removal and baseline extraction modules to obtain absorbance spectra from distorted dual-comb absorption spectroscopy. The etalon removal module utilizes a typical U-net model, and the baseline extraction module consists of a modified U-net model with physical constraint and an adaptive iteratively reweighted penalized least squares method serving as refinement. The training datasets combine experimental baselines and simulated gas absorption with different concentrations, fully exploiting prior information on gas absorption features from the HITRAN database. In the simulated and experimental test, the CO_2 absorbance spectrum covering 25 cm^{-1} shows high consistency with the HITRAN database, of which the mean absolute error is less than 1% of the maximum absorbance value, and the retrieved concentration has a relative error under 2%, outperforming traditional approaches and indicating the potential practicality of our data processing framework. Hopefully, with a larger network volume and proper datasets, this processing framework can be extended to precise quantification analysis in more comprehensive applications such as atmospheric measurement and industrial monitoring.

Keywords

Dual-comb absorption spectroscopy, deep learning, etalon removal, baseline extraction, absorbance spectra quantification analysis

Date received: 28 June 2023; accepted: 7 December 2023

Introduction

Dual-comb absorption spectroscopy (DCAS) has emerged as a promising and powerful technique in gas absorption spectroscopy, which provides broad spectral coverage, high resolution, high acquisition speed, and frequency accuracy,[1] leading to wide applications ranging from open-path atmospheric monitoring[2,3] through combustion diagnosis[4,5] to hyperspectral imaging.[6,7] Combining the advantages of both laser and broadband spectroscopy, DCAS has provided far richer gas information than conventional gas detection approaches, for example, tunable diode laser absorption spectroscopy.[8] However, this technique is still confronted with some challenges in obtaining absorbance spectra and performing quantitative analysis to recover gas parameters under different circumstances. For one thing, the etalon effects caused by optical components,[2,4,9] which is common in laser spectroscopy, could distort normal spectrum, especially in weak absorption conditions when the amplitude of sine fringe is comparable with that of gas absorption. For another, both the complex baseline from comb sources and complicated gas absorption in broadband spectroscopy could impair the baseline extraction,[10,11] causing poor results in absorbance spectrum. Therefore, advanced approaches to achieve etalon removal and baseline extraction are essential and critical for DCAS.

[1]State Key Laboratory of Precision Measurement Technology & Instruments, Department of Precision Instrument, Tsinghua University, Beijing, China
[2]School of Instrumentation Science and Opto-Electronics Engineering, Beihang University, Beijing, China

Corresponding Author:
Haoyun Wei, State Key Laboratory of Precision Measurement Technology & Instruments, Department of Precision Instrument, Tsinghua University, Beijing 100084, China.
Email: luckiwei@mail.tsinghua.edu.cn

In DCAS, etalon effects are traditionally discouraged by optical path adjustment, which could make optical components designment or researcher operation more complex[12–14] and few algorithms have been conducted on this problem. Meanwhile, two primary baseline extraction approaches are commonly employed in DCAS: Direct baseline measurement supported by additional hardware and post-processing using algorithms. As for the former, it is conventionally carried out by measuring a reference spectrum without target absorption,[12,15] which could add complexity to the hardware system and still suffers from intensity fluctuation with minor changes in optical path. Besides, in open-path or combustion measurement circumstances, a reference spectrum without target absorption is more difficult to achieve. The latter is piecewise fitting (PWF) the DCAS with polynomial parts and gas absorption parts using the HITRAN database.[2,16] Yet this approach is ineffective in coping with complex baselines and etalon fringes, and the high-order polynomial could increase the degree of freedom in the fitting processing, which could cause more deviation from real baseline and absorbance spectrum. Apart from the approaches in DCAS above, there are additional baseline extraction methods in other spectroscopy techniques, such as adaptive iteratively reweighted penalized least squares (airPLS)[17] and polynomial iteration (PI).[18] The fundamental premise of these methods is that non-absorbing regions exist in the spectrum; therefore, in the densely or broadly absorbed region, the retrieved baseline could induce lower absorbance results. To diminish the error induced by baseline, some researchers also proposed baseline-free approaches for DCAS, which mainly focus on time-domain signals, though careful optical path adjustment or complex fitting algorithm is needed.[10,19]

Over the past few years, deep learning, which makes giant strides in image and natural language processing,[20–22] has drawn increasing attention in one-dimension spectroscopy processing, such as spectroscopy denoising,[23,24] classification,[25,26] and prediction.[27] In addition, some researchers also introduce deep learning in undesirable signal removal, such as removing non-resonant background from coherent anti-stokes Raman scattering signal[28] and eliminating cosmic ray and background signal in Raman spectra[29] using a convolution neuron network model. Further, deep learning also contributes to baseline extraction using an adversarial model[30] or a U-net model,[31] and the results show that deep learning models have a better performance than traditional baseline extraction methods. Inspired by previous spectroscopy data processing research and the potential capacity of deep learning, it is appealing to remove etalon effects and achieve complex baseline extraction with advanced deep learning model in DCAS.

Here, a novel deep learning enabled data processing framework for distorted DCAS is proposed in which DCAS with etalon effects is the input and the absorbance spectrum is the final output. In this framework, a typical U-net model is utilized to remove etalon effects, mitigating the distortion of spectra and the baseline is obtained by combining a modified U-net that suits the physical constraint in gas absorption with traditional airPLS method serving as refinement. Both deep learning models are trained with datasets using simulated gas absorption from HITRAN database, which will exclusively help the network distinguish etalon effects or complex baseline from DCAS. The simulation and experiment results show that our data processing framework can recover high-fidelity absorbance spectra which are feasible for subsequent quantitative analysis, proving its potential to be employed in the data processing of various applications in DCAS. It can also be extended to different gases with a corresponding training set derived from HITRAN database and broader spectral coverage with a larger volume in the deep learning model.

Experimental Theory

DCAS Data Processing Framework

Optical frequency comb is consecutive pulses with fixed repetition rate in the time domain and evenly separated comb teeth covering several hundreds of wavenumbers in the frequency domain. When passing through the sample, the comb light is encoded with gas molecular response. Using a second comb with slight difference in repetition frequency to perform asynchronous optical sampling, as shown in Figure 1a, a radio frequency comb containing the gas molecular response is generated by the heterodyne beats between pairs of comb teeth. Two configurations, depending on whether one or two combs pass through the gas sample, namely asymmetric and symmetric configuration, are common in DCAS applications. In the asymmetric configuration, the amplitude and phase spectra can be fully obtained, while in the symmetric configuration, only amplitude spectra with double gas absorption are available. Notably, the absorbance spectra derived from interference signal of asymmetric DCAS configuration are half that derived from light intensity signal of traditional laser absorption spectroscopy techniques.

In the context of DCAS, for one thing, etalon effects are common as there are some optical planar components inside the comb source or in the optical measurement path, like beam splitters and optical windows. When the period or the amplitude of the sine-like fringes are comparable with gas absorption features, it could be more difficult to differentiate normal gas absorption features from original DCAS, and subsequent baseline extraction results could suffer from more deviation due to the disturbance from etalon effects. Thus, as shown in Figure 1b, in the DCAS data processing framework, the etalon removal module containing a typical U-net deep learning model is initially used to remove the etalon effects in the spectrum. For another, dense or broad gas

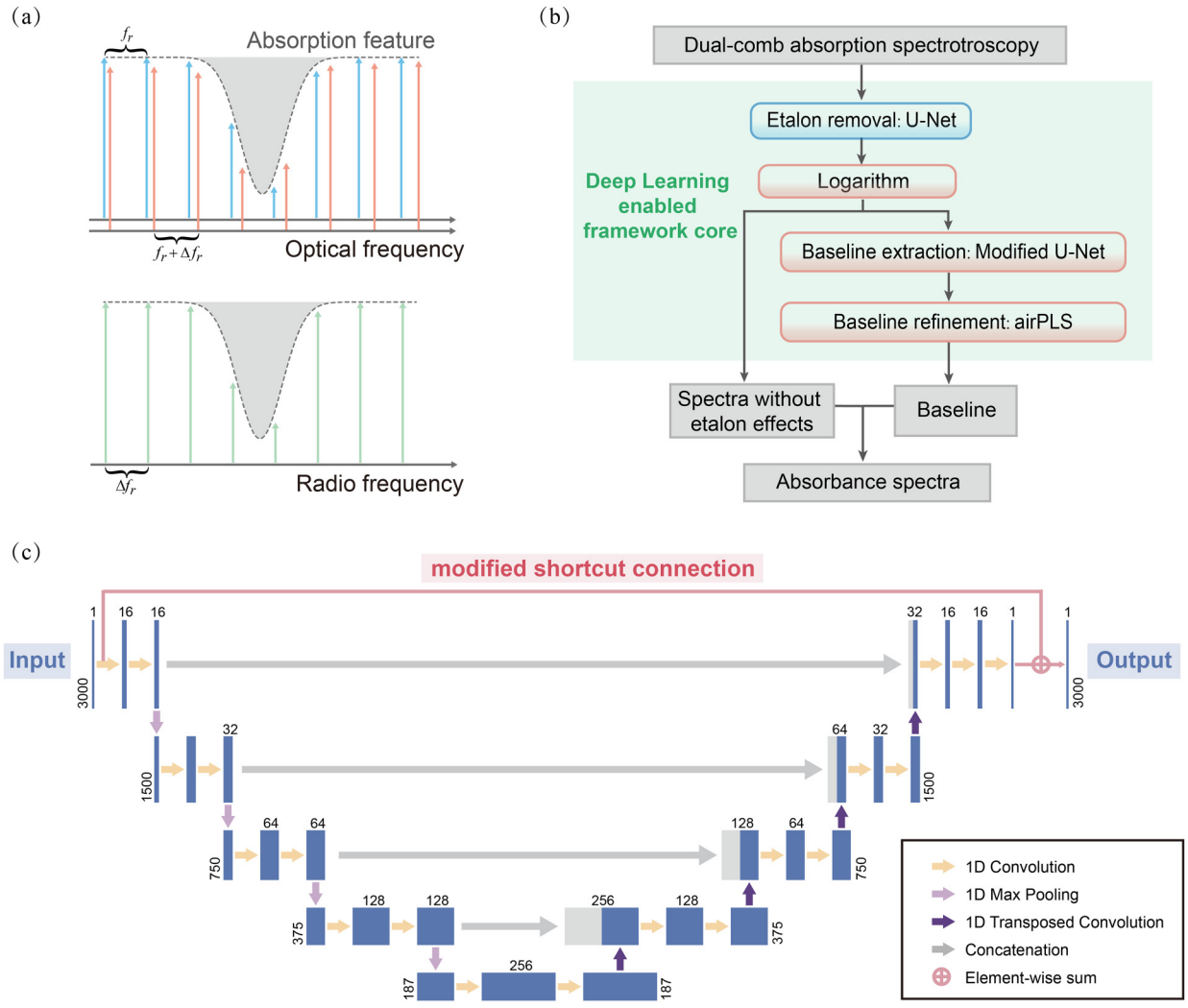

Figure 1. (a) The principle of dual-comb absorption spectroscopy. (b) The framework of the dual-comb absorption spectroscopy data processing. (c) Structure of the etalon removal network (typical U-net model) and the baseline extraction network (modified U-net model).

absorption could make no non-absorbing region existing in a broad spectra range, which could add complexity to baseline extraction algorithm of broadband spectroscopy. Besides, due to the nonlinear optical process inside the comb source and the optical interference process in the heterodyne detection, the baseline of DCAS is more complex than traditional broadband spectroscopy. Therefore, another module of our deep learning enabled framework core, namely baseline extraction module, is set to address this issue. In this module, the spectrum after etalon removal is performed by the logarithmic operation and sent to a modified U-net model which suits the physical constraint in gas absorption to extract a preliminary baseline. Then, a refinement step using airPLS method is employed to recover a more accurate baseline. Finally, the absorbance spectrum is obtained by normalizing the spectrum after logarithmic operation with the final baseline.

Etalon Removal Module

The U-net model, containing an encoder and decoder with concatenation between them, has wide applications in biomedical image segmentation.[32] Here, we choose a typical one-dimensional (1D) U-net model in etalon removal module to separate etalon effects from distorted spectra.

As shown in Figure 1c, the network structure comprises four down-sampling stages to extract features and four up-sampling stages to expand data in the encoder and decoder. Apart from these, there are concatenation stages between every down-sampling and up-sampling stage, which is crucial for U-net model to deliver data features. Every down-sampling stage has two 1D convolutional layers, each of which has a convolution kernel of three with a stride of one and is followed by a parametric rectified linear unit and a batch normalization. A max pooling layer with a kernel of two is employed between two stages in down-sampling

path. Every up-sampling stage also has two one-dimension convolutional layers with the same configuration as that in down-sampling stages, and a one-dimension transposed convolution layer is employed between two stages in up-sampling path.

In the etalon removal module, the input and output of the network is DCAS with and without etalon effects. Both the input and output vector have a size of 1×3000, and the sizes of feature vector in the whole process are labeled in Figure 1c.

To train this etalon removal network, we use synthetic data combining simulated gas absorption and experimental baseline with etalon effects. The detailed dataset generation approach is below. First, we obtain original baselines with etalon effects from our previous DCAS system,[33] which is normalized by their corresponding maximum value. Second, smoothness operation is carried out to eliminate sinusoidal fringes and to generate target baselines without etalon effects. Next, the baseline data is inverted to increase the dataset. Then the original and target baseline is multiplied with transmittance function of target gas with different concentration based on Beer–Lambert law to generate input and target dataset. According to the approach above, a total number of 40 000 samples are randomly generated, of which 80% are used for training set and 10% for validation set and 10% for testing set. It is worth mentioning that to achieve a good performance of etalon removal, etalon features of specified dual-comb spectrometer should be involved in training set and this process of dataset preparation is applicable.

The network was trained for 100 epochs and a mini-batch size of 256. Adaptive moment estimation (Adam) algorithm is chosen to perform the optimization with a mean squared error (MSE) loss function and the learning rate of 0.001.

Baseline Extraction Module

In Beer–Lambert law, the spectra transmittance intensity $I_t(\nu)$ has the following relationship with baseline $I_0(\nu)$:

$$I_t(\nu) = I_0(\nu)\exp[-\alpha(\nu)L] \tag{1}$$

where $\alpha(\nu)$ denotes the gas absorption coefficient, and L denotes the optical path. From Eq. 1, it can be seen that separating baseline and gas absorption features from $I_t(\nu)$ is complex due to the multiplicative and exponential relationship. Therefore, to alleviate the difficulty of distinguishing gas absorption features and baseline in neural network, we take the logarithm of Eq. 1 to obtain:

$$\ln[I_0(\nu)] = \ln[I_t(\nu)] + \alpha(\nu)L \tag{2}$$

Based on this addition relationship, we develop a physical constraint network using a modified U-net model, as shown in Figure 1c, which adds a shortcut connection between the input and output. This unique connection forces the network to concentrate more on the gas absorption features compared to previous baseline extraction deep learning model.[30,31]

To train this baseline extraction network, we use synthetic data combining simulated gas absorption and experimental baselines after smoothness operation. The detailed dataset generation approach is below. First, we choose the baselines which have been smoothed in the Etalon Removal section above. Second, transmission intensity is simulated based on Beer–Lambert law using gas absorption coefficient of different concentration and different baseline. Third, we add random noises whose amplitude is 1% of the maximum signal to the transmission intensity to simulate the SNR in our DCAS system. Finally, to meet the physical constraint in this modified U-net model, a logarithm operation on transmission intensity and baseline is employed, generating input and target dataset. According to the approach above, a total number of 40 000 samples are randomly generated, of which 80% are used for training set and 10% for validation set and 10% for testing set.

Considering the smoothness property of baseline, we add a smoothness regularization term to the MSE loss function:

$$\text{Loss} = \frac{1}{n}\|y' - y\|_2 + m\left(\frac{1}{n}\sum_k |\boldsymbol{y}(k+1) - \boldsymbol{y}(k)|\right) \tag{3}$$

where y and y' denote the output and target of the network, and n denotes the length of the input vector, and m denotes the regularization parameter. In the process of network training, we finally set m to 0.01 as the validation set has a lower residual error under condition of this value.

AirPLS, an approach that has been widely used in baseline correction in Raman spectroscopy, is applicable to signals containing baseline information. Detailed deduction can be inferred from Zhang et al.,[17] and we only give a concise introduction here. In penalized least squares method with weight, the objective function comprises the fidelity with weight and penalties on the roughness, which can be given by:

$$Q = (y - z)^{\mathrm{T}} W (y - z) + \lambda (Dz)^{\mathrm{T}} (Dz) \tag{4}$$

where y denotes the original signal vector, and z denotes the baseline. W is the weighted matrix with w_i on its diagonal, and D is the difference matrix. The balance between fidelity and smoothness can be achieved by tuning λ. By equating the partial derivative to 0, the baseline vector can be obtained by:

$$z = (\boldsymbol{W} + \lambda \boldsymbol{D}^{\mathrm{T}} \boldsymbol{D})^{-1} \boldsymbol{W} y \tag{5}$$

In the adaptive iteratively reweighted procedure, the w_i in iterative step k is expressed as:

$$w_i^k = \begin{cases} 0 & y_i \le z_i^{k-1} \\ \exp[k(y_i - z_i^{k-1})/|\boldsymbol{d}^k|] & y_i > z_i^{k-1} \end{cases} \tag{6}$$

where vector d^k denotes the positive elements of the differences between y and z^{k-1}, and the iteration will stop either when maximal iteration time or threshold of $|d^k|$ is reached.

After using the modified U-net to extract preliminary baseline, majority of the elements in the output have been recovered to the true baseline, while some elements still deviate from the target baseline. To address this issue, we choose airPLS method to refine our baseline extraction results exploiting the fact that some baseline information has been recovered in the modified U-net model.

Simulation Results

To demonstrate this dual-comb framework, we choose carbon dioxide as the target gas in the spectral range of 6349 to 6374 cm^{-1}, in which dense and strong absorption from carbon dioxide makes no non-absorbing region exist. The spectra data contain 3000 points, corresponding to 250 MHz spectral resolution for our dual-comb source. And for a specified dual-comb spectrometer application, the number of points could be set arbitrarily to meet the desired spectral range and spectral resolution of comb sources. Meanwhile, a new training dataset and training process are needed to complete the network model applicable for this dual-comb spectrometer application.

Shown in Figures 2a and 2b are two etalon removal cases in the test set. It can be seen that before processing by the network (red curve), sinusoidal fringes distort original gas absorption signals of carbon dioxide, while after etalon removal, the distortions are suppressed, making true gas absorption more straightforward. Normalized by the ideal baseline, we obtain absorbance residual of two cases compared with standard absorbance spectra. The sinusoidal fringes with varying amplitude are evident in the absorbance residual of input results and are weakened apparently in that of output results, and the mean absolute values (MAEs) are $2.7\times10^{-3}/9.7\times10^{-4}$ (input/output) and $3.9\times10^{-3}/1.5\times10^{-3}$, respectively. Figures 2c and 2d give the spectrum analysis of absorbance residual, in which the normalized frequency is defined as the frequency normalized by half of the sampling frequency. The spectrum results reveal significant suppression of the etalon-induced frequency features after the network with the suppression ratio of 11.7 and 4.7 for two cases, verifying the availability of this network model. In addition, we provide another example that two stimulated etalons of different frequencies distort the absorption spectroscopy in Supplemental Material, and Figure S1 has

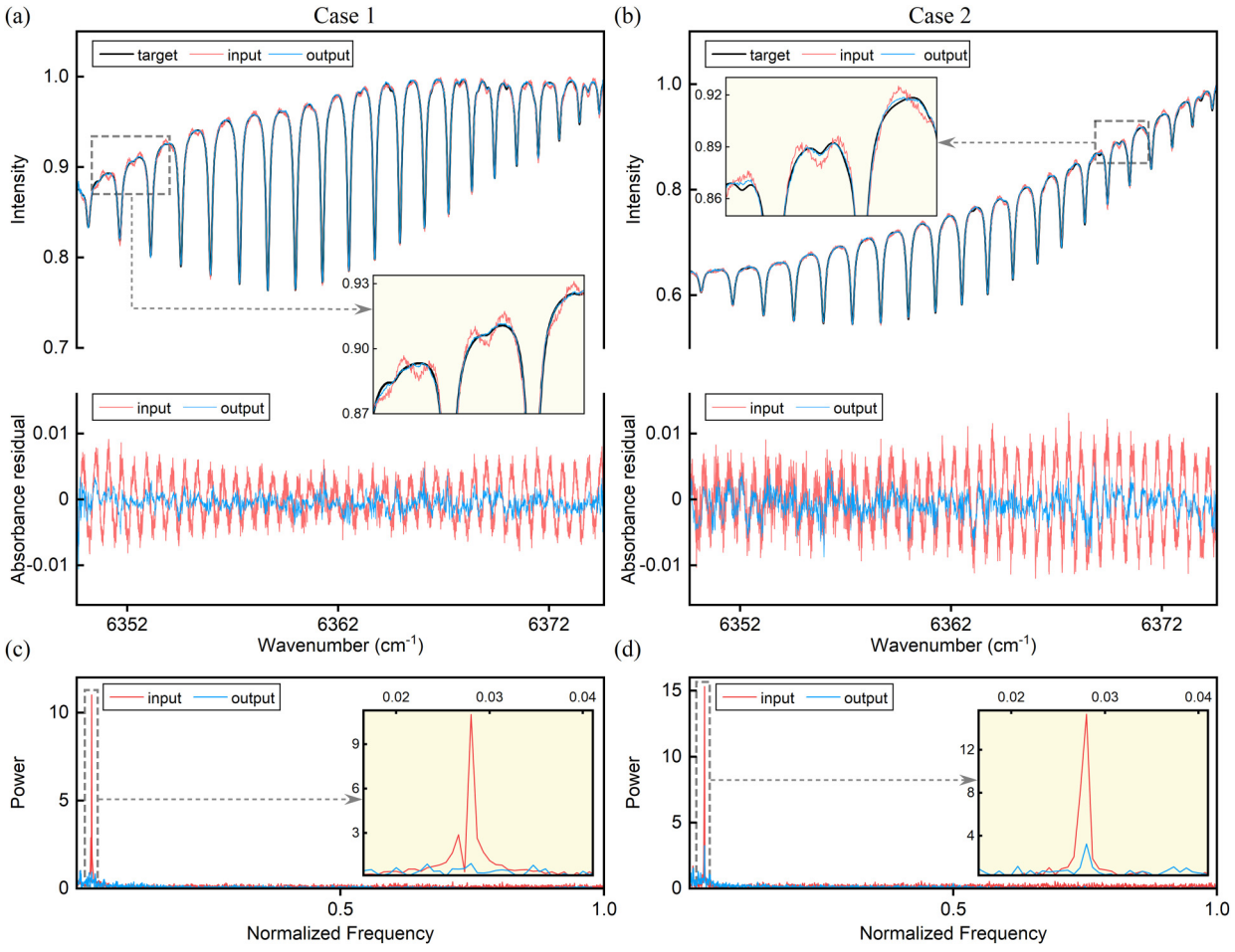

Figure 2. (a, b) Etalon removal results of case 1 and case 2. (c, d) The spectrum of absorbance residual of case 1 and case 2.

shown good performance of suppression of two etalon features, proving the applicability for multiple etalons removal of this network model.

The simulation results of modified U-net output and refinement by smoothness operation or airPLS method are shown in Figures 3a and 3b. The smoothness refinement is a normal smoothing operation using moving averaging method with a span of 50, whereas airPLS refinement is a more aggressive operation exploiting the recovered baseline information from the output of the modified U-net, of which the smoothness parameter λ is 10^7.The MAEs of them for case I/case II are $1.4\times10^{-3}/1.2\times10^{-3}$, $1.3\times10^{-3}/1.1\times10^{-3}$, and $4.9\times10^{-4}/4.6\times10^{-4}$, respectively. It is apparent in the insets that the direct output of modified U-net still suffers from some deviation, and simply smoothness operation cannot indeed diminish it while using airPLS method as refinement can recover a baseline with lower residual. In addition, we have compared baseline extraction performance of traditional methods (yellow, blue, and green curve) and deep learning enabled module (combining modified U-net and airPLS refinement method, red curve) in Figures 3c and 3d. In this comparison, for traditional methods, we empirically choose reasonable parameters to reach their best performance. For airPLS, the smoothness parameter λ is 10^7; for PI, the polynomial is seventh-order, and the iteration repeats for 100 times; for PWF, the fitting is conducted by a sixth-order polynomial baseline across 150 GHz windows. The MAEs of them for case I/case II are $1.5\times10^{-2}/1.4\times10^{-2}$, $1.1\times10^{-2}/1.0\times10^{-2}$, $3.4\times10^{-3}/8.8\times10^{-4}$, and $4.9\times10^{-4}/4.6\times10^{-4}$, respectively. The true concentrations for case I/case II are 100/92%, and the concentrations retrieved from the absorbance spectra based on four different baselines are 82.63/76.52%, 87.27/80.79%, 95.90/88.83%, and 99.75/91.28%, corresponding to relative errors of 17.37/16.82%, 12.73/12.18%, 4.10/3.45%, and 0.25/0.78%, respectively. The comparison results prove that baseline extraction plays a vital role in the quantification analysis, and our deep learning enabled module outperforms traditional methods. In the Supplemental Material, we also provide another baseline extraction example of formic acid in the mid-infrared range to verify its applicability for broadband absorption features.

Figures 4a and 4b show the absorbance spectra output (red curve) of the data processing framework, whose inputs are shown in Figure 2 as red curve. The overall outputs are in good accordance with the absorbance from HITRAN database (red curve) with MAEs of 1.1×10^{-3} and 1.6×10^{-3} for two cases, respectively, though some weak absorption peaks are diminished in the region around 6363 cm^{-1}, as shown in the inset of Figure 4b. The retrieved concentration is 78.50% and 94.66% while the true values are 78% and 95%, corresponding to relative errors of 0.64% and 0.36%, respectively. We also use the PWF approach which is common in DCAS to obtain the absorbance spectra, as shown in Figures 4c

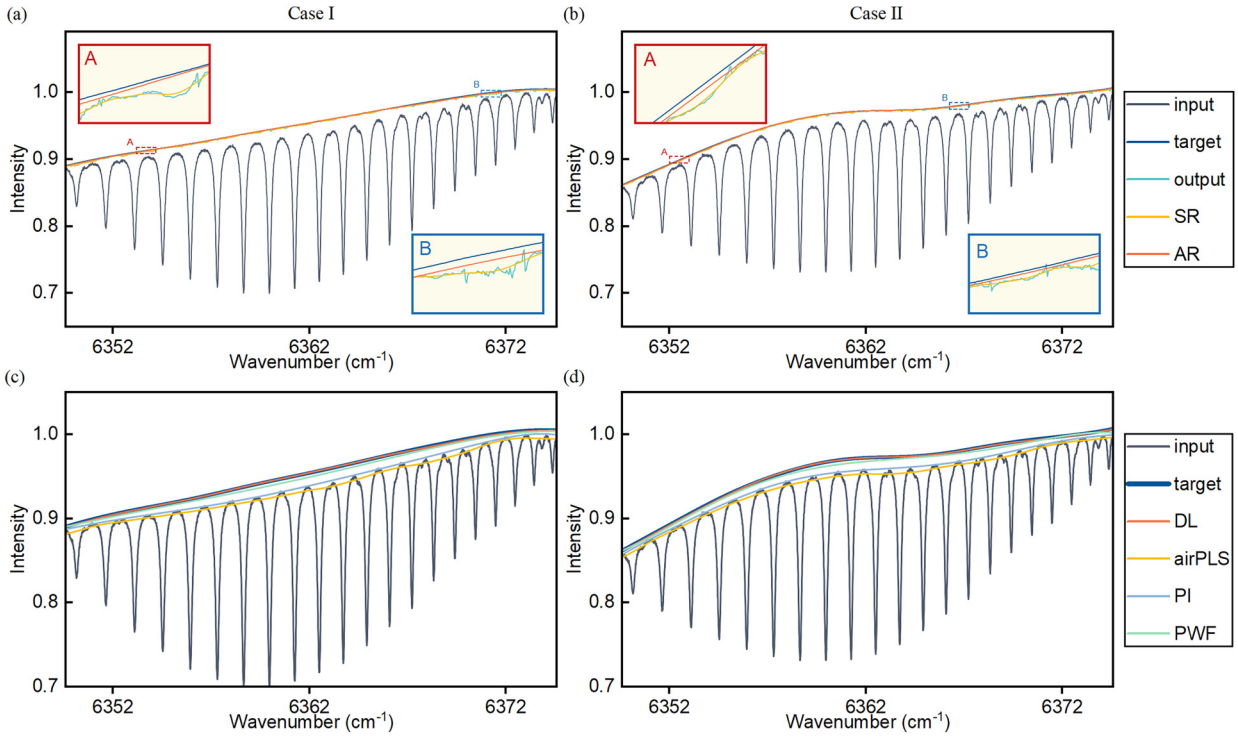

Figure 3. (a, b) Comparison of different refinement methods in deep learning enabled module (SR: smoothness refinement, AR: airPLS refinement). (c, d) Baseline extraction simulation results of deep learning enabled module and traditional methods (airPLS: adaptive iteratively reweighted penalized least squares, PI: polynomial iteration, PWF: piecewise fitting).

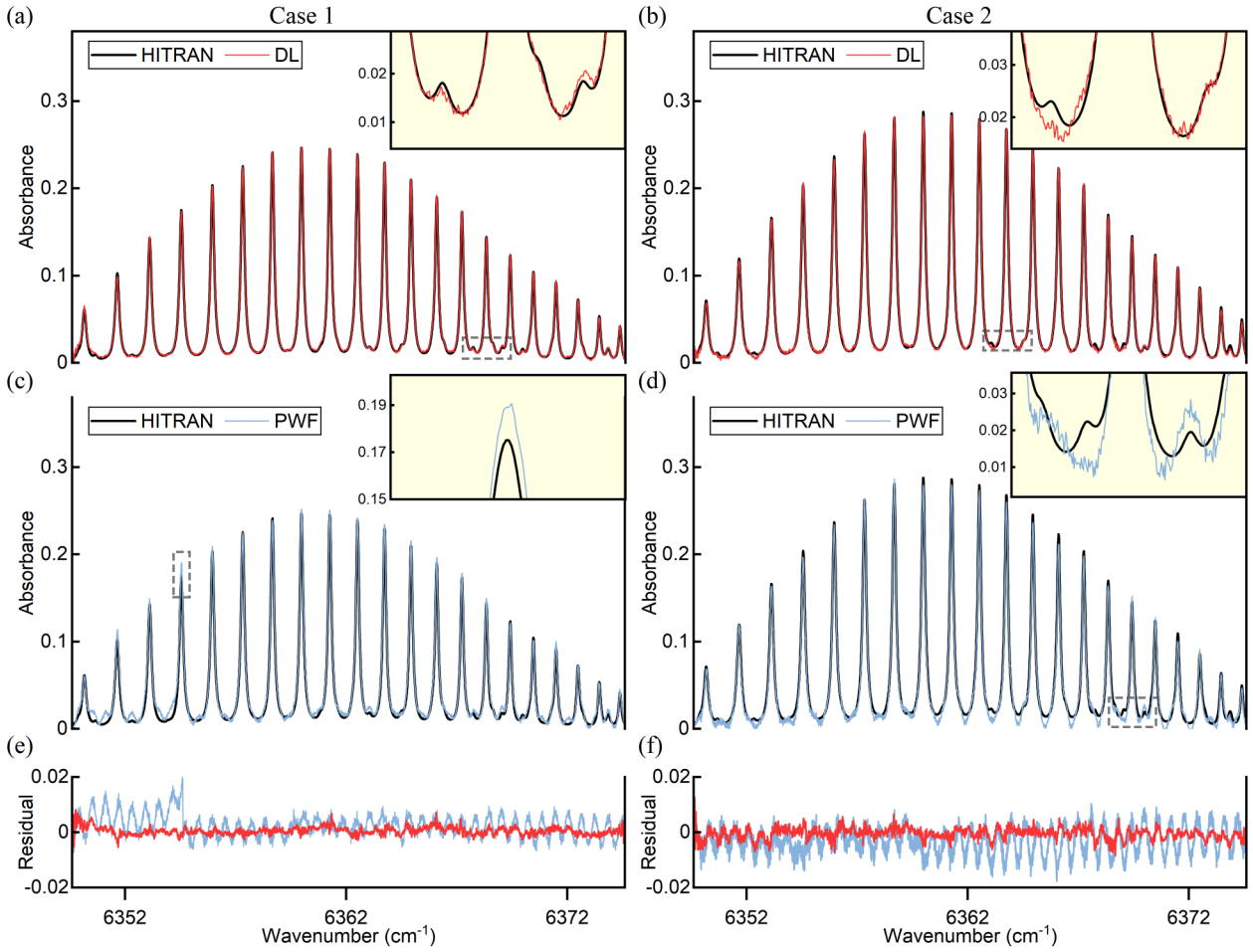

Figure 4. (a, b) The simulation results of case 1 and case 2 using the deep learning enabled approach. (c, d) The simulation results of case 1 and case 2 using piecewise fitting approach. (e, f) Absorbance residual of case 1 and case 2 for two approaches.

and 4d. The MAEs of the absorbance spectra are 3.6×10^{-3} and 4.7×10^{-3} for two cases, about three times higher than deep learning enabled approach, which is visible in absorbance residual shown in Figures 4e and 4f. The retrieved concentrations are 80.75% and 91.00% for two cases, with the relative errors of 3.52% and 4.21%, respectively, much higher than that of deep learning enabled approach.

To sum up, the simulation results demonstrate that the data processing framework is suitable for DCAS and has better performance than traditional approaches. Besides, the computational time for etalon removal network and baseline extraction network are about 16.0 and 16.3 ms on NVIDIA Quadro P2000, indicating the feasibility of the data processing framework.

Experimental

Materials and Methods

The scheme of our DCAS system setup is shown in Figure 5a. Two independent near-infrared fiber optical combs centered around 1550 nm operate at a repetition rate of 250 MHz with the difference of the repetition rate of 230 Hz. Two combs have an asymmetric configuration, in which comb 1 serves as a local comb and comb 2 is the signal comb. The output light from comb 2 is first collimated by a collimator to pass through a 2 m long gas cell filled with CO_2 and then coupled into fiber by another fiber coupler. Then the signal comb light encoded by gas response is divided into two parts. One part combines with the light from comb 1 to generate interferograms at the detector while the other part is sent to optical beat processing. To suppress the noises from comb sources themselves and turbulence in the measurement optical path, we choose two continuous-wave (CW) diode lasers centered at 1534.22 and 1564.70 nm as reference light sources to extract signals containing noise information as dual-compensation method described in Chen et al.[34] Beat processing module has four input optical signals, including the light from comb 1, the light from comb 2 after passing the gas cell and the light from two CWs, which outputs four electronic signals generated by beating between two pairs of combs and CWs. Then the acquisition system will simultaneously record the four

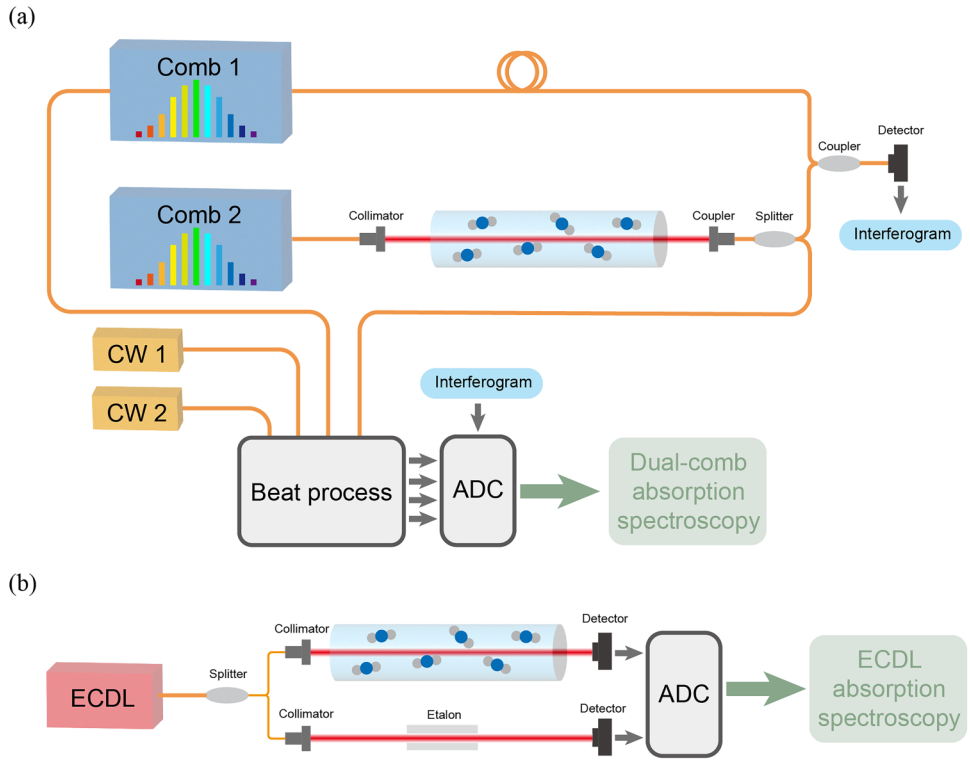

Figure 5. (a) The experiment setup of dual-comb absorption spectroscopy measurement system. (b) The experiment setup of external cavity diode laser absorption spectroscopy measurement system.

electronic signals from beat processing module and one interferogram signal from the detector. Finally, the acquired signals are processed to produce the corrected interferograms free from noises of both comb sources and optical path, and to obtain corresponding DCAS after Fourier transform.

To verify our absorbance spectra measurement results, a near-infrared external cavity diode laser (ECDL), which has a scan range from 1520 to 1630 nm, is employed to measure the absorbance spectra of the gas cell as shown in Figure 5b. The light from ECDL is divided into two parts, one of which passes through the gas cell and another through a silicon etalon to record its relative scan wavelength. It is worth noting that the baseline of ECDL spectroscopy is measured in the same optical path before filling the gas cell with CO_2.

Results and Discussion

The CO_2 absorption spectroscopy measured by the DCAS system, which is the result of coherent averaging for 30 s, is shown in Figure 6a. It is clear that the CO_2 absorption features are distorted by etalon effects, especially in the region around 6372 cm^{-1}. Using the ECDL system with measured baseline, absorbance spectrum can be obtained, and the fitted concentration is 99.26%, which is regarded as the standard concentration in subsequent absorbance spectra comparison. The absorbance spectrum processed by deep learning enabled approach is shown as red curve in Figure 6b. Some weak absorption peaks in the middle region have been recovered properly, while that in the margin region suffer from more deviation, probably caused by the misidentification in etalon removal network. As for the strong absorption peaks, they are all clearly recovered and the large deviation around 6356 cm^{-1} is presumably attributed to the over-estimation in baseline extraction module. Compared with standard absorbance from the HITRAN database, the MAE of the retrieved absorbance is 1.35×10^{-3}, less than 1% of the maximum absorbance value. Additionally, to perform quantification analysis, the concentration retrieved from DCAS system is 97.30%, with a relative error of 1.97%, indicating that our processing framework for DCAS has a good performance in etalon removal and baseline extraction function and are available for subsequent quantification analysis.

To further validate the advantages of our deep learning enabled approach, a comparison with the traditional PWF approach is conducted. To obtain the good performance of PWF approach, we divide the spectrum into five parts to piecewise fit with a sixth-order polynomial and the result is shown as blue curve in Figure 6c. Compared with the result of deep learning enabled approach, it is clear that the absorbance spectrum is subjected to far more deviation as this traditional approach cannot handle the etalon effects, and its fitted baseline could distort significantly in the region around 6372 cm^{-1}, where the etalon effects obviously degrade the

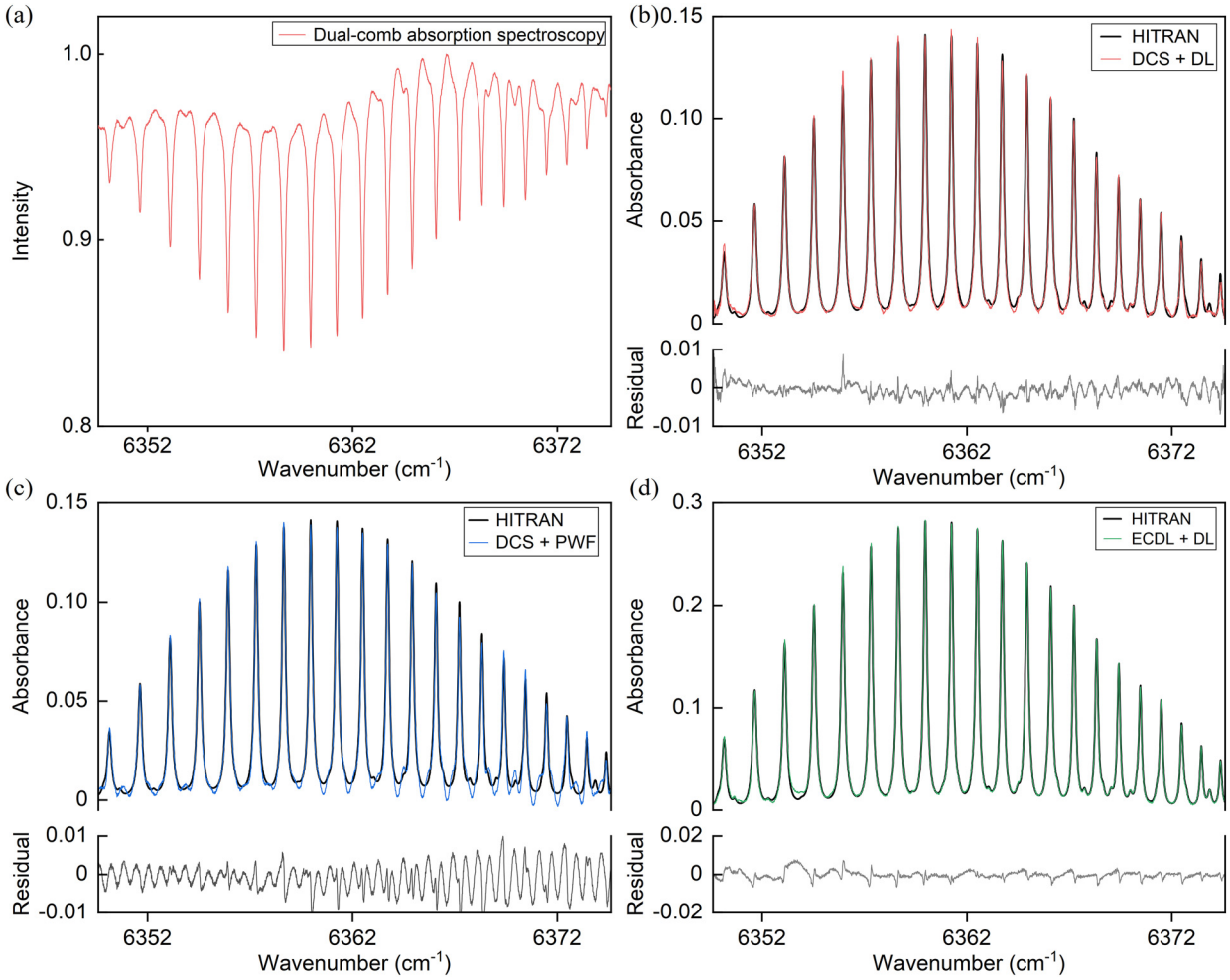

Figure 6. (a) Experimental result of dual-comb absorption spectroscopy. (b) Absorbance spectrum from DCAS system using deep learning enabled data processing framework. (c) Absorbance spectrum from DCAS system using piecewise fitting approach. (d) Absorbance spectrum from ECDL system with deep learning enabled baseline.

gas absorption features. In quantitative comparison, the MAE of the absorbance retrieved by PWF is 2.9×10^{-3}, and the recovered concentration is 95.93% with a relative error of 3.35%, both of which are higher than that of deep learning enabled approach, verifying that the deep learning enabled approach could recover more high-fidelity absorbance spectra and is more conducive to quantification analysis than traditional PWF approach.

Moreover, we test the baseline extraction module performance in the ECDL absorption spectroscopy. To satisfy the input requirement for the modified U-net model, we have resampled the ECDL spectra data covering 6349 to 6374 cm^{-1} to a vector of 3000 points in advance. As shown in Figure 6d, the absorbance spectrum result derived from deep learning enabled baseline is in good agreement with standard absorbance, with the MAE of 1.51×10^{-3}, and the line errors around absorption peaks could be attributed to the minor errors in the process of wavelength calibration. The concentration retrieved from this absorbance spectrum is 98.62%, with a relative error of 0.64%, which further validates the practicality for our baseline extraction module.

Conclusion

In conclusion, we have proposed a novel deep learning enabled dual-comb spectroscopy data processing framework in this paper. Two major components, including etalon removal and baseline extraction modules, are designed to address the etalon effects problems and the difficulty in extracting complex baseline from dense or broad gas absorption regions. The etalon removal module uses a U-net model, and the baseline extraction module consists of a modified U-net model with physical constraint and an airPLS method serving as refinement. The training is performed on datasets developed by combining experimental baselines and simulating gas absorption with different concentrations, fully exploiting prior information of gas absorption features from HITRAN database. The performance of the data processing

framework is assessed on CO_2 absorbance spectra measurement based on our DCAS system, and the results indicate that our data processing framework can recover the target absorbance spectra from the original spectra distorted by etalon effects in no non-absorption region and outperform traditional approaches. Additionally, the concentration retrieved from the recovered absorbance spectra has a relative error of less than 2%, further demonstrating the great potential for facilitating quantification analysis. Though limited by the network input, a spectral bandwidth covered just 25 cm^{-1} is displayed in this paper, larger spectral coverage for broadband absorption is also promising with the increase of network volume. Besides, training datasets derived from the HITRAN database and aimed at different pure or mixed gases can also extend the data processing framework to various applications in DCAS, such as open-path monitoring and combustion diagnosis.

Declaration of Conflicting Interests

The authors declared no potential conflicts of interest with respect to the research, authorship, and/or publication of this article.

Funding

The authors disclosed receipt of the following financial support for the research, authorship, and/or publication of this article: This work was supported by the National Natural Science Foundation of China (Grant No. 62275138).

ORCID iD

Chao Huang https://orcid.org/0009-0005-1207-8256

Supplemental Material

All supplemental material mentioned in the text is available in the online version of the journal.

References

1. I. Coddington, N. Newbury, W. Swann. "Dual-Comb Spectroscopy". Optica. 2016. 3(4): 414–426.
2. G.B. Rieker, F.R. Giorgetta, W.C. Swann, J. Kofler, et al. "Frequency-Comb-Based Remote Sensing of Greenhouse Gases Over Kilometer Air Paths". Optica. 2014. 1(5): 290–298.
3. F.R. Giorgetta, J. Peischl, D.I. Herman, G. Ycas, et al. "Open-Path Dual-Comb Spectroscopy for Multispecies Trace Gas Detection in the 4.5–5 μm Spectral Region". Laser Photonics Rev. 2021. 15(9): 2000583.
4. A.S. Makowiecki, D.I. Herman, N. Hoghooghi, E.F. Strong, et al. "Mid-Infrared Dual Frequency Comb Spectroscopy for Combustion Analysis from 2.8 to 5 μm". Proc. Combust. Inst. 2021. 38(1): 1627–1635.
5. P.J. Schroeder, R.J. Wright, S. Coburn, B. Sodergren, et al. "Dual Frequency Comb Laser Absorption Spectroscopy in a 16 Mw Gas Turbine Exhaust". Proc. Combust. Inst. 2017. 36(3): 4565–4573.
6. P. Martín-Mateos, F.U. Khan, O.E. Bonilla-Manrique. "Direct Hyperspectral Dual-Comb Imaging". Optica. 2020. 7 (3): 199–202.
7. E. Vicentini, Z. Wang, K. Van Gasse, T.W. Hänsch, N. Picqué. "Dual-Comb Hyperspectral Digital Holography". Nat. Photonics. 2021. 15(12): 890–894.
8. G.B. Rieker, J.B. Jeffries, R.K. Hanson. "Calibration-Free Wavelength-Modulation Spectroscopy for Measurements of Gas Temperature and Concentration in Harsh Environments". Appl. Opt. 2009. 48(29): 5546–5560.
9. E. Baumann, E.V. Hoenig, E.F. Perez, G.M. Colacion, et al. "Dual-Comb Spectroscopy with Tailored Spectral Broadening in Si3n4 Nanophotonics". Opt. Express. 2019. 27(8): 11869–11876.
10. R.K. Cole, A.S. Makowiecki, N. Hoghooghi, G.B. Rieker. "Baseline-Free Quantitative Absorption Spectroscopy Based on Cepstral Analysis". Opt. Express. 2019. 27(26): 37920–37939.
11. G. Ycas, F.R. Giorgetta, J.T. Friedlein, D. Herman, et al. "Compact Mid-Infrared Dual-Comb Spectrometer for Outdoor Spectroscopy". Opt. Express. 2020. 28(10): 14740–14752.
12. G. Ycas, F.R. Giorgetta, E. Baumann, I. Coddington, et al. "High-Coherence Mid-Infrared Dual-Comb Spectroscopy Spanning 2.6 to 5.2 Mm". Nat. Photonics. 2018. 12(4): 202–208.
13. A.D. Draper, R.K. Cole, A.S. Makowiecki, J. Mohr, et al. "Broadband Dual-Frequency Comb Spectroscopy in a Rapid Compression Machine". Opt. Express. 2019. 27(8): 10814–10825.
14. R.K. Cole, A.D. Draper, P.J. Schroeder, C.M. Casby, et al. "Demonstration of a Uniform, High-Pressure, High-Temperature Gas Cell with a Dual Frequency Comb Absorption Spectrometer". J. Quant. Spectrosc. Radiat. Transfer. 2021. 268: 107640.
15. G. Ycas, F.R. Giorgetta, K.C. Cossel, E.M. Waxman, et al. "Mid-Infrared Dual-Comb Spectroscopy of Volatile Organic Compounds Across Long Open-Air Paths". Optica. 2019. 6 (2): 165–168.
16. K.C. Cossel, E.M. Waxman, F.R. Giorgetta, M. Cermak, et al. "Open-Path Dual-Comb Spectroscopy to an Airborne Retroreflector". Optica. 2017. 4(7): 724–728.
17. Z. Zhang, S. Chen, Y. Liang. "Baseline Correction Using Adaptive Iteratively Reweighted Penalized Least Squares". Analyst. 2010. 135(5): 1138.
18. C.A. Lieber, A. Mahadevan-Jansen. "Automated Method for Subtraction of Fluorescence from Biological Raman Spectra". Appl. Spectrosc. 2003. 57(11): 1363–1367.
19. T. Tomberg, A. Muraviev, Q. Ru, K.L. Vodopyanov. "Background-Free Broadband Absorption Spectroscopy Based on Interferometric Suppression with a Sign-Inverted Waveform". Optica. 2019. 6(2): 147–151.
20. K. He, X. Zhang, S. Ren, J. Sun. "Deep Residual Learning for Image Recognition". Paper presented at: 2016 IEEE Conference on Computer Vision and Pattern Recognition (CVPR). Las Vegas, Nevada; 27–30 June 2016.
21. A. Krizhevsky, I. Sutskever, G.E. Hinton. "Imagenet Classification with Deep Convolutional Neural Networks". Commun. ACM. 2017. 60(6): 84–90.
22. I. Sutskever, O. Vinyals, Q.V. Le. "Sequence to Sequence Learning with Neural Networks". Paper presented at: 28th Annual Conference on Neural Information Processing Systems (NIPS 2014). Montreal, Canada; 8–13 December 2014.

23. C.C. Horgan, M. Jensen, A. Nagelkerke, J.-P. St-Pierre, et al. "High-Throughput Molecular Imaging via Deep-Learning-Enabled Raman Spectroscopy". Anal. Chem. 2021. 93(48): 15850–15860.
24. Y. Zhang, M. Lu, J. Hu, Y. Li, et al. "Rapid Coherent Raman Hyperspectral Imaging Based on Delay-Spectral Focusing Dual-Comb Method and Deep Learning Algorithm". Opt. Lett. 2023. 48(3): 550–553.
25. C.-S. Ho, N. Jean, C.A. Hogan, L. Blackmon, et al. "Rapid Identification of Pathogenic Bacteria Using Raman Spectroscopy and Deep Learning". Nat. Commun. 2019. 10 (1): 4927.
26. J. Hu, Y. Zou, B. Sun, X. Yu, et al. "Raman Spectrum Classification Based on Transfer Learning by a Convolutional Neural Network: Application to Pesticide Detection". Spectrochim. Acta, Part A. 2022. 265: 120366.
27. K. Ghosh, A. Stuke, M. Todorović, P.B. Jørgensen, et al. "Deep Learning Spectroscopy: Neural Networks for Molecular Excitation Spectra". Adv. Sci. 2019. 6(9): 1801367.
28. C.M. Valensise, A. Giuseppi, F. Vernuccio, A. De La Cadena, et al. "Removing Non-Resonant Background from Cars Spectra Via Deep Learning". APL Photonics. 2020. 5(6): 061305.
29. J. Wahl, M. Sjödahl, K. Ramser. "Single-Step Preprocessing of Raman Spectra Using Convolutional Neural Networks". Appl. Spectrosc. 2020. 74(4): 427–438.
30. Y. Liu. "Adversarial Nets for Baseline Correction in Spectra Processing". Chemom. Intell. Lab. Syst. 2021. 213: 104317.
31. T. Chen, Y. Son, A. Park, S.-J. Baek. "Baseline Correction Using a Deep-Learning Model Combining Resnet and Unet". Analyst. 2022. 147(19): 4285–4292.
32. O. Ronneberger, P. Fischer, T. Brox. "U-Net: Convolutional Networks for Biomedical Image Segmentation". In: N. Navab, J. Hornegger, W.M. Wells, A.F Frangi, editors. Medical Image Computing and Computer-Assisted Intervention (MICCAI 2015), 18th International Conference, Munich, Germany; 5–9 October 2015. Lecture Notes in Computer Science. Switzerland: Springer International Publishing, 2015. Vol. 9351, Pp. 234–241.
33. W. Zhang, X. Chen, X. Wu, Y. Li, H. Wei. "Adaptive Cavity-Enhanced Dual-Comb Spectroscopy". Photon. Res. 2019. 7(8): 883–889.
34. X. Chen, C. Huang, J. Li, M. Lu, et al. "Phase-Sensitive Open-Path Dual-Comb Spectroscopy with Free-Running Combs". Phys. Rev. Appl. 2023. 19(4): 044016.